Chapter 3
Diffusion Sensitive Magnetic Resonance Imaging of the Central Nervous System

Jeffrey J. Neil and Joseph J.H. Ackerman

Abstract Diffusion magnetic resonance (MR) imaging offers a wealth of information on the physiologic condition and microstructure of the brain. This chapter starts with a description of the fundamentals of MR and MR diffusion measurements. This is followed by descriptions of: (1) the role of water apparent diffusion coefficient measurements in detecting tissue injury, (2) the use of diffusion anisotropy measurements to assess the development of and injury to cerebral cortex and white matter, and (3) diffusion-based measurements of white matter connections ("tractography"). The chapter concludes with a brief summary of the utility of measurement of diffusion of molecules other than water in the central nervous system.

Keywords Magnetic resonance imaging • Diffusion • Diffusion tensor imaging • Diffusion tractography • Axial diffusivity • Radial diffusivity

3.1 Introduction

In the main, magnetic resonance imaging (MRI) detects the ^{1}H ("proton") nuclear magnetic resonance (NMR) signal from water. While other substances and other nuclides are NMR active, only water is present at sufficient concentration in mammalian tissue

J.J. Neil, M.D., Ph.D. (✉)
Departments of Pediatric Neurology, Pediatrics and Radiology,
Washington University School of Medicine, 660 South Euclid Ave.,
St. Louis, MO 63110, USA
e-mail: neil@wustl.edu

J.J.H. Ackerman, Ph.D.
Departments of Chemistry, Radiology and Internal Medicine, Campus Box 1134,
Washington University, 1 Brookings Drive, St. Louis, MO 63130, USA
e-mail: ackerman@wustl.edu

I.-Y. Choi and R. Gruetter (eds.), *Neural Metabolism In Vivo*,
Advances in Neurobiology 4, DOI 10.1007/978-1-4614-1788-0_3,

to provide the strong signal strength required for routine, robust, time-efficient, imaging applications. Thus, MRI is different from many other imaging modalities, such as positron emission tomography (PET), single photon emission computerized tomography (SPECT), and most applications of optical imaging, in that it does not detect an exogenously administered tracer species but rather the 100% naturally abundant ^{1}H in endogenous tissue water.

Within the medical community, the adjective "nuclear" in "NMR" is generally dropped to form the more politically correct "MR". Importantly however, "nuclear" refers to the fundamental quantum mechanical origin of the phenomenon; specifically, stimulated energy level transitions among different states of nuclear spin (states of different nuclear angular momentum). When placed in a static magnetic field, these nuclear spin states possess different energies and stimulated transitions between these states (between different energy levels) result in detectable absorption or emission of energy.

In marked distinction to the more familiar nuclear disintegration reactions exploited in PET and SPECT, for which very high energy particles are given off as the nucleus of a given isotope decays to form a new isotope, nuclear spin transitions are of extremely low energy, typically in the radio frequency range. Energies in this range are essentially harmless to living systems. Indeed, we are bathed in radio frequency waves emanating from radio, TV, and cell-phone transmissions. Further, static magnetic fields and radio frequency waves readily penetrate most non-metallic objects. Thus, the MR phenomenon is fundamentally noninvasive and nondestructive to living systems, including human.

The low energy nuclear spin states couple weakly to their surrounding environment (formally, to the "lattice"). This results in a particular advantage. Once the spins are perturbed from their thermal equilibrium energy level population distribution, it takes a long time before the thermal equilibrium distribution is reestablished. This return to a state of thermal equilibrium is referred to as "relaxation" and MR relaxation times are very long compared to other familiar spectroscopies. For example, while tissue water ^{1}H MR relaxation times dependend upon tissue type and physiologic state, typical MR relaxation times are on the order of 10–1000 ms (1 ms $=10^{-3}$ s), far longer than optical relaxation times which are measured in nano-, pico-, and even femtoseconds (10^{-9} to 10^{-15} s). A long relaxation time is advantageous because it is precisely during this time when the spins are out of equilibrium that spatial coordinate information is encoded and the image formed. Longer relaxation times confer greater precision in spatial encoding, resulting in the exceptionally clear anatomic definition characteristic of MRI.

The long relaxation times also allow many physical properties of tissue water to be encoded on a voxel by voxel basis in the MR image intensity (contrast generation). For example, images can be created that map water content, blood flow velocity, volumetric perfusion rate, tissue elasticity (stress and strain), tissue displacement, neuronal activation, oxygen extraction fraction, and temperature. Images can also be created in which contrast is determined by the tissue relaxation times. Two relaxation times are most relevant. The exponential relaxation time constant governing the disappearance of the MR signal is referred to as T_2. T_2-weighted contrast typically provides exceptional anatomical definition and is a mainstay of clinical MRI exams.

The exponential relaxation time constant governing reestablishment of the thermal equilibrium spin-state energy-level population distribution is referred to as T_1. T_1-weighted images are often used in concert with administration of exogenous T_1 relaxation agents (contrast agents) to monitor vascular permeability, perfusion, and blood brain barrier integrity. Contrast enhanced T_1-weighted images are a mainstay of oncologic MRI exams.

Another physical property of tissue water, its incoherent displacement motion or diffusion, can be encoded in the MR image and forms the subject of this chapter. The thermal energy present in tissue at 37°C manifests itself in the form of random, incoherent displacements of individual water molecules. These thermally driven stochastic displacements, characteristic of all liquids, are referred to as Brownian motion in honor of Robert Brown, the English botanist who discovered the phenomenon in 1827 upon observing with a microscope the jostling of pollen grains suspended in water. The ongoing, ever continuing, random displacement jumps occur for every member of the vast collection of water molecules that occupy each MR image voxel. The displacement jumps occur with very high frequency, such that molecular collisions occur at a staggering rate. Considering pure water, for example, the rotational correlation time – the average time between two collisions for a given water molecule, collisions which change rotational state – is on the order of 10^{-12} s; put another way, the average water molecule experiences 10^{12} collisions per second. These molecular collisions result in a random walk of all water molecules, i.e., diffusion, even for systems at thermal equilibrium. The net result of this diffusive motion is that, over time, all members of a collection of water molecules move throughout the accessible space. Such an effect can be readily mimicked by carefully placing a small drop of red dye in the center of a beaker of still water. Over time the region of dye grows larger in size (while becoming more dilute) and slowly spreads to the boundaries of the beaker. This is diffusive motion.

Over the typical time scale accessible to the diffusion-sensitive MRI experiment (t_{diff}), 1–100 ms, water diffusion leads to average (root-mean-square, $<X^2>^{1/2}$) displacements of 1–10 μm. This scale matches well with the microarchitectural structural features characteristic of mammalian tissue. These microstructural elements (cell and organelle membranes, for example) serve to hinder and restrict the diffusion of tissue water. Thus, the MRI diffusion experiment serves to probe tissue microstructure and, importantly, changes therein due to physiologic and pathophysiologic challenge. For this reason, diffusion sensitive MRI has become a powerful clinical and preclinical research tool.

When carried out in quantitative fashion, the MRI diffusion experiment results in maps of the apparent diffusion constant (ADC), the coefficient of proportionality between the average displacement distance and time, Eq. 3.1. The term "apparent" is used because the analysis usually employs a mathematics that is strictly true only for free (unhindered, unrestricted) diffusion, a condition clearly violated for water diffusion in tissue.

$$\sqrt{\left\langle X^2 \right\rangle} \propto \sqrt{ADC \times t_{diff}} \tag{3.1}$$

The MR encoding of water diffusion employs the same three-axis (x, y, z) magnetic field gradient coils used for anatomic spatial encoding. It follows that it is possible to encode for the diffusion of water along any direction in the laboratory frame of reference by application of the appropriate combination of x-, y-, and z-axis magnetic field gradients. Indeed, for each voxel in an image it is possible to encode the entire diffusion tensor. The diffusion tensor describes the three dimensional diffusion properties of tissue water in a local (voxel-based diffusion-oriented) coordinate frame of reference. In the example of the hypothetical small drop of red dye placed in the middle of a beaker of water, the tendency of the dye to diffuse along any particular direction would be the same as there is no directional preference to diffusive displacement. Likewise, if the MR ADC was determined along different directions for water in the beaker, the result would always be the same. Diffusion in this situation is isotropic (lacks directional preference). But this is not always the case.

Instead of a large beaker of water with a small drop of red dye in its center, consider a long and very narrow glass capillary filled with water. The diffusive motion of water along the axis of the capillary tube is completely unrestricted and unhindered. The ADC measured along this axis would be exactly the same as that measured along any direction in a large beaker of water. However, the same is clearly not true for diffusion measured along a direction radial (orthogonal) to the capillary axis. Here the glass walls of the tube present an impenetrable boundary to diffusion, the displacement motion of water is restricted, and diffusion "appears" slow. Indeed, no matter how long one waits, i.e., no matter how long t_{diff} is, water never appears outside the glass capillary. Thus, ADC_{radial} is much less than ADC_{axial}, and ADC_{radial} appears to decrease as the time allowed for diffusion, t_{diff}, increases. This hypothetical situation is one in which there is extreme diffusion anisotropy, a strong directional preference. Were the water MR diffusion tensor obtained in this case, it would provide (1) the orientation of the capillary tube in the laboratory reference frame (i.e., the angles defining the local coordinate frame – the three eigenvectors) and (2) the two ADCs (ADC_{axial} and ADC_{radial}).

Water diffusion in a narrow glass capillary is not only anisotropic but possesses cylindrical symmetry. Here the measurement of ADC along any direction orthogonal to the capillary axis would yield the same value. While water diffusion in mammalian tissue is often found to be anisotropic, the MR diffusion tensor experiment does not necessarily assume cylindrical symmetry. Indeed, as usually applied, three eigenvectors (ν_1, ν_2, ν_3) and three eigenvalues (λ_1, λ_2, λ_3) are obtained. As noted above, the eigenvectors define the local (voxel-based diffusion coordinate) frame of reference and the three eigenvectors are the ADCs ("diffusivities") along each axis defined by the eigenvectors: λ_1 is the ADC along ν_1, λ_2 is the ADC along ν_2, and λ_3 is the ADC along ν_3. Generally the diffusivities are ordered as $\lambda_1 > \lambda_2 > \lambda_3$. In the special case of cylindrical symmetry, ν_1 defines the axial orientation of the cylinder and λ_1 is the diffusivity along the axis of the cylinder, often written as $\lambda_{\parallel}$ and read as "lamda parallel" or "axial diffusivity". Further, for this special case, $\lambda_2 = \lambda_3$ and both are generally written as $\lambda_{\perp}$ and read as "lamda perpendicular" or "radial diffusivity". In practice, water in mammalian tissues rarely presents a case of pure cylindrical

symmetry although approximate cylindrical symmetry is not unusual: $\lambda_1 >> \lambda_2 \sim \lambda_3$. Here the average of λ_2 and λ_3 is taken as the radial diffusivity, i.e., $(\lambda_2 + \lambda_3)/2 = \lambda_\perp$.

Full diffusion tensor imaging presents the problem of displaying the six parameters derived for each voxel (ν_1, ν_2, ν_3, λ_1, λ_2, λ_3) in a single image. Numerous schemes employing color (RBG) and geometrical shapes (diffusion probability ellipsoids) are in use, but will not be reviewed here. However, it is very common to display maps representing the extent of diffusion anisotropy by collapsing the three diffusivities (λ_1, λ_2, λ_3) into a single "summary" parameter, typically either the fractional anisotropy or the relative anisotropy (Armitage and Bastin 2000). Fractional anisotropy (FA) is calculated as follows,

$$FA = \frac{\sqrt{3}}{\sqrt{2}} \frac{\sqrt{(\lambda_1 - \lambda)^2 + (\lambda_2 - \lambda)^2 + (\lambda_3 - \lambda)^2}}{\sqrt{\lambda_1^2 + \lambda_2^2 + \lambda_3^2}}, \tag{3.2}$$

where λ is the average diffusivity, $(\lambda_1 + \lambda_2 + \lambda_3)/3$. Relative anisotropy (RA) is calculated as

$$RA = \frac{1}{\sqrt{6}} \frac{\sqrt{(\lambda_1 - \lambda)^2 + (\lambda_2 - \lambda)^2 + (\lambda_3 - \lambda)^2}}{\lambda}. \tag{3.3}$$

Both summary parameters seek to represent as a single value, the voxel intensity, the difference between the individual diffusivities and their average. The way in which this works is most readily seen by considering two special cases: isotropic diffusion and diffusion in a long very narrow cylinder (the capillary tube).

In the case of isotropic diffusion $\lambda_1 = \lambda_2 = \lambda_3$; thus there is no difference between the individual diffusivities and their average, λ. In practice, noise in the MR measurement prevents the situation where $\lambda_1 = \lambda_2 = \lambda_3$ is found (i.e., there is a noise floor that prevents observation of pure isotropic diffusion by MR). Nevertheless, where diffusion tensor MR finds that water diffusion is well approximated as isotropic, $\lambda_1 \sim \lambda_2 \sim \lambda_3$, the FA or RA would be small and the voxel intensity would be low. In the case of diffusion in a long and very narrow cylinder (the capillary tube), $\lambda_1 > \lambda_2$, $\lambda_3 \sim 0$; thus, there is a substantial difference between the individual diffusivities and their average, λ. As a result, their FA or RA would be large, and the voxel intensity would be high. It follows therefore that FA or RA maps are bright where tissue water diffusion is anisotropic and dark where water diffusion is isotropic. In this manner, the information contained within the full diffusion tensor is compressed into an easily displayed gray scale. However, the true values of the diffusivities and the orientation of the local diffusion frame are lost.

Two final summary parameters worth noting are the sum and the average of the principal diffusivities (λ_1, λ_2, λ_3). The sum $(\lambda_1 + \lambda_2 + \lambda_3)$ is referred to as the trace of the tensor. The average, λ, is referred to as the mean ADC, i.e., the directionally averaged ADC. If we take the tensor to be represented by an ellipsoidal geometric shape, the orientation of the ellipsoid is given by the three eigenvectors (ν_1, ν_2, ν_3),

and the shape of the ellipsoid (rugby ball vs. pancake; long, narrow vs. short, squat; etc.) is given by the length of its axes (λ_1, λ_2, λ_3). Here the trace or mean ADC is seen to reflect the overall size of the ellipsoid (large vs. small rugby ball) independent of its relative dimensions or orientation. Again, employing the trace or mean ADC is a way to compress the information contained within the full diffusion tensor into an easily displayed gray scale. Here bright voxels indicate that tissue water diffusion is, on average, fast, while dark voxels indicate that, on average, diffusion is slow. In this compression scheme, all directional information about water diffusion has been lost.

In summary, MR diffusion measurements exploit and quantify the diffusion of water as a means to infer characteristics of the underlying structural microarchitecture that hinders and restricts the thermally driven stochastic molecular motion of water. The MR "diffusion signal" thus provides information on a spatial scale far smaller than that of normal image voxel dimensions, μm vs. mm. As many tissues present significant structural ordering on the micron scale, the MR diffusion signal has proven extremely powerful in characterizing normal, abnormal, and developing morphology and physiology.

3.2 Information Available Through Diffusion Imaging: ADC

ADC values are typically calculated as the average of the three eigenvalues. The most common clinical application of diffusion imaging is for the acute evaluation of brain injury. As shown in Fig. 3.1, the decrease in ADC values that accompanies stroke serves as an early indicator of brain injury (Moseley et al. 1990), with changes in diffusion images visible within minutes of the onset of injury. In contrast, ischemic injury may not be detectable for days on conventional MR imaging. ADC values decrease following a variety of central nervous system insults in addition to stroke,

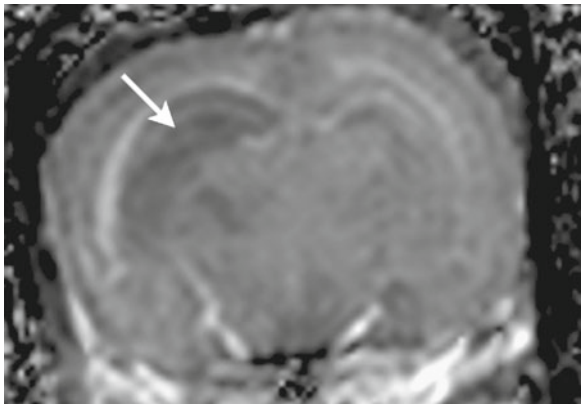

Fig. 3.1 A coronal ADC map from a live, 3.2-g mouse pup taken 24 h after common carotid ligation and 45 min of hypoxia. Darker areas denote lower ADC values. Note the area of injury (*arrow*) which primarily affects the neuronal cell layer of the hippocampus (Image provided courtesy of Drs. Tim West and Greg Lodygensky)

including status epilepticus (Zhong et al. 1993), excitotoxic injury (Dijkhuizen et al. 1999), spreading depression (Busch et al. 1995; Rother et al. 1996; Takano et al. 1996) and trauma (Ito et al. 1996). Thus, a decrease in ADC is a nonspecific finding. In addition, changes in ADC values are sometimes reversible. For example, cerebral vascular occlusion causes local water ADC values to decrease within minutes. If blood flow is restored before permanent injury occurs, ADC values return to normal (Li et al. 1999). Similarly, the decrease in ADC induced by the application of excitotoxins can be reversed by blocking the excitotoxin receptor (Dijkhuizen et al. 1999).

The reduction in ADC values following stroke is not 100% sensitive on the first day after injury. In adults with stroke, for example, the incidence of "diffusion-negative" injury is on the order of 6% (Schlaug et al. 1997; Oppenheim et al. 2000). In newborn infants, the incidence may be as high as 30% (McKinstry et al. 2002b). The explanation for this finding is likely related to the nature of the injury. In animal studies, transient cerebral vascular occlusion (30 min), which is sufficient to cause permanent injury, leads to a delayed decrease in ADC values (Li et al. 2000; Lin et al. 2001; Dijkhuizen et al. 1998). Under these circumstances, ADC values are reduced during occlusion, but return to normal when blood flow is restored. ADC values then decrease again over a time period of approximately 24 h, reaching a nadir at 2 to 4 days after injury. In this case, diffusion imaging does not identify the area of injury for up to 24 h. In contrast, permanent cerebral vascular occlusion leads to a sustained decrease in ADC values within minutes of occlusion. The circumstances of cerebral injury to a newborn infant may be more similar to the animal model of transient occlusion. Infants who are experiencing hypoxia in utero are often delivered quickly by caesarean section, after which blood flow and oxygenation are restored. Vascular occlusion in adults with stroke, on the other hand, lasts for 24–48 h, more closely approximating permanent occlusion. Thus, the mechanism of cerebral injury affects the evolution of diffusion image contrast, even though both injuries result in permanent cerebral infarction.

It should also be kept in mind that ADC values vary with time after injury. As noted above, ADC values reach a nadir at 2 to 4 days after injury and then gradually return to normal over a time period of approximately 1 week – a process known as "pseudonormalization" (Schlaug et al. 1997; Copen et al. 2001; Mukherjee et al. 2000; McKinstry et al. 2002b). After pseudonormalization, ADC values are higher than normal in the area of injury and remain so. Thus, the sensitivity of diffusion measurements for detecting injury varies markedly with time after injury. Overall, the decrease in ADC values is most sensitive for detecting stroke 2 to 4 days after injury, though the majority of injury in adults and children is detectable within minutes of its occurrence.

The biophysical mechanisms behind the decrease in tissue ADC after injury are not well understood. The most-commonly cited (and likely incorrect) hypothesis for the cause of this change is the compartment shift hypothesis. This explanation is based on the assumption that water in the intra- and extracellular spaces has different ADC values – high for extracellular water and low for intracellular water. If water in these two compartments is in fast exchange, the measured overall tissue ADC is a weighted average of the ADC values for water in these two compartments.

When cells swell in response to injury, the proportion of water in the intracellular space increases at the expense of water in the extracellular space. This causes heavier weighting of the overall ADC to that of water in the intracellular compartment, leading to a decrease in the overall tissue water ADC value. While this hypothesis is attractive, the evidence for its validity remains indirect and weak, resting primarily on the close temporal relationship between the injury-induced decrease in water ADC and cell swelling. Estimates of ADC values for water in the intra- and extracellular compartments suggest that their ADC values are not sufficiently different for a shift of water from the extra- to intracellular space to account for the decrease in ADC associated with injury (Duong et al. 1998; Silva et al. 2002). As an alternative hypothesis, some authors have suggested that a decrease in the ADC of intracellular water is responsible for the ADC drop (Neil et al. 1996; Wick et al. 1995). This remains an area of active debate.

The change in water ADC associated with brain injury is not universal, but does occur in other tissues. In skeletal muscle, for example, the decrease in water ADC values following injury is much smaller than that in brain (Heemskerk et al. 2006). In kidney, on the other hand, ADC values decrease following ischemia (Liu and Xie 2003). Similarly, ADC values fall quickly and significantly in prostate following injury caused by heating or cooling (Butts et al. 2003). In addition, diffusion MR methods hold promise for evaluating tumors (Hamstra et al. 2005; Moffat et al. 2006).

ADC values can also increase acutely with some forms of pathology, particularly vasogenic edema. Reversible posterior leukoencephalopathy syndrome (RPLS) is an example. This condition is associated with a variety of clinical conditions, including hypertension or the administration of chemotherapeutic agents (Hinchey et al. 1996). It is characterized by mental status changes, visual disturbance, headache, and seizures. The MRI findings include abnormality of the occipital lobes, with increased ADC values. The change in ADC values has been attributed to vasogenic edema and an increase in the volume of the extracellular space with an associated reduction in the restriction of water displacement. In this case, diffusion tensor imaging is useful for differentiating RPLS from occipital stroke, as stroke is associated with a decrease in ADC values (Ay et al. 1998).

3.3 Information Available Through Diffusion Imaging: Anisotropy

3.3.1 White Matter

In mature brain, anisotropy values are typically higher from regions of white matter (WM) than grey matter (GM), as shown in Fig. 3.2. Further, anisotropy is often taken as representative of the "health" of a white matter tract. One of the first research groups to apply anisotropy in this fashion (Klingberg et al. 2000), showed that diffusion anisotropy in the left temporo-parietal WM was strongly correlated with

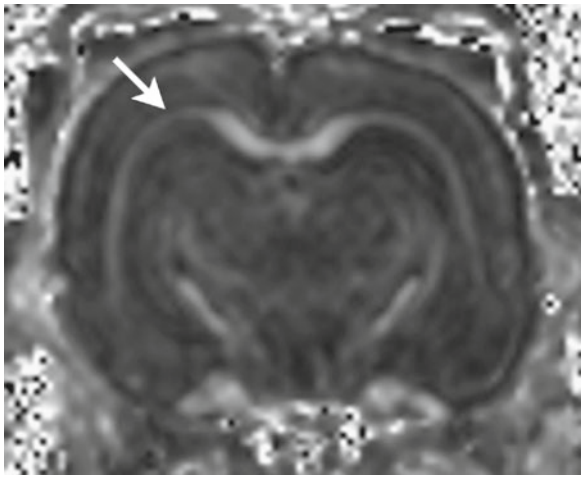

Fig. 3.2 A coronal anisotropy map from a 9-day-old rat pup. Brighter areas denote higher anisotropy. Note that anisotropy values are higher in white matter areas, particularly the corpus callosum and external capsule (*arrow*) (Image provided courtesy of Dr. Greg Lodygensky)

reading scores. This study spawned a series of reports comparing WM anisotropy values to clinical conditions such as schizophrenia, though the validity of such studies remains controversial (Kanaan et al. 2005). The precise relationship between anisotropy and WM health is not yet understood, nor is it clear what parameter (e.g., tract size, anisotropy value) would serve as the best indicator in this application. Despite these limitations, WM diffusion anisotropy measurements are a valuable measure for evaluation of WM diseases such as multiple sclerosis (Goldberg-Zimring et al. 2005).

A more sophisticated approach to evaluating anisotropy data from WM involves analysis of the eigenvalues. The eigenvalue for λ_1, referred to as "axial diffusivity," represents water ADC parallel to axons. The average of the eigenvalues for λ_2 and λ_3, referred to as "radial diffusivity," describes water ADC perpendicular to axons. Data from animal studies show that primary injury to myelin is associated with an increase in radial diffusivity, presumably because there are fewer myelin membranes to hinder water displacements in this direction. Conversely, primary injury to axons, such as Wallerian degeneration, is associated with a decrease in axial diffusivity, presumably because of disruption of the fiber tracts along which water molecules can diffuse (Song et al. 2002, 2005; Sun et al. 2006).

Finally, anisotropy measurement can be applied to evaluation of white matter maturation and injury, particularly in prematurely-born infants, for whom white matter abnormality is common (Woodward et al. 2006). During normal white matter development, the increase in anisotropy takes place in two stages. Surprisingly, the initial increase occurs before the presence of histologically-detectable myelin. This increase has been attributed to changes in axonal structure associated with the pre-myelinating state and has been detected in both animals (Wimberger et al. 1995) and humans (Huppi et al. 1998; Neil et al. 1998). It is followed by a second, larger increase in anisotropy associated with the elaboration of layers of myelin (Mukherjee et al. 2002). Thus, measurement of anisotropy can be used for evaluating aberrant white matter development as well as injury (Neil et al. 2002).

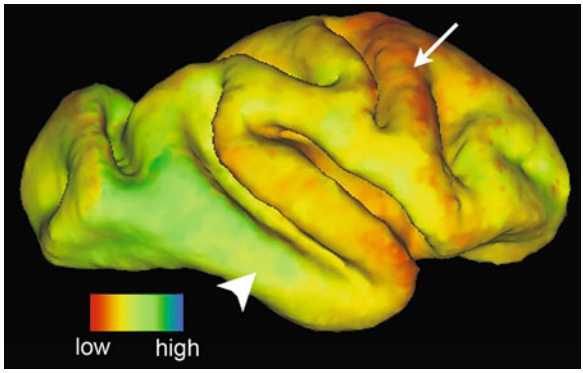

Fig. 3.3 A surface representation of a baboon hemisphere at 125 days gestation (term gestation is 185 days). The color scale shows cortical anisotropy values. Note the heterogeneity of cortical development, with the precentral gyrus appearing more mature (*arrow*, lower anisotropy) than the inferior temporal area (*arrow head*, higher anisotropy)

3.3.2 Grey Matter

In adult brain, anisotropy values from cortical GM are typically low and relatively uninteresting. However, cortical anisotropy values are high during the early stages of cortical development, such as during brain development of prematurely-born human infants, providing information on cortical development. This has been shown in both human (McKinstry et al. 2002a) and animal (Kroenke et al. 2007) studies. Anisotropy values are transiently high during early development because of the radial orientation of apical dendrites of pyramidal cells. This confers larger water displacements orthogonal to the cortical surface than parallel to it. As development progresses, anisotropy values decrease due to the addition of interneurons and elaboration of basal dendrites of pyramidal cells. An example of high cortical anisotropy during cortical development is shown in Fig. 3.3.

3.4 Information Available Through Diffusion Imaging: Tractography

The primary eigenvector, λ_1, is oriented parallel to the orientation of fiber tracts for white matter. As shown in Fig. 3.4, it is possible to follow fiber tracts within the brain by tracking the orientation of this eigenvector from voxel to voxel (Conturo et al. 1999; Xue et al. 1999; Basser et al. 2000). This application of diffusion imaging has not yet seen widespread clinical use, but one potential application is for planning neurosurgical procedures. It may be possible to determine where crucial white matter tracts lie in relation to tumors. This knowledge might be used to alter the neurosurgical approach, helping to minimize the neurologic deficits associated with tumor resection.

One challenge for diffusion tractography is tracking crossing fibers. The tensor formalism presented here is the earliest, and most widely-used, means of representing water displacements in three dimensions. It continues to serve well in a variety

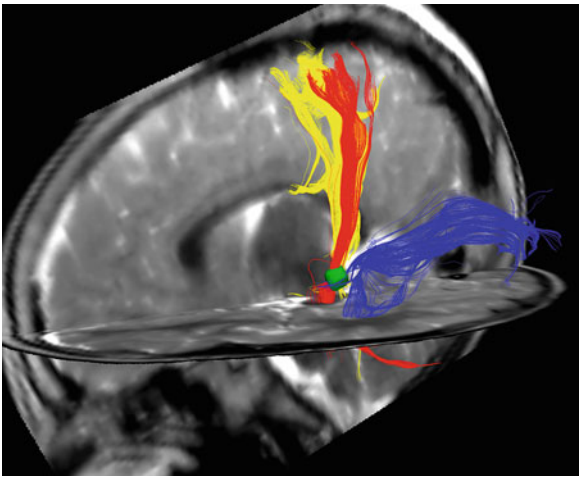

Fig. 3.4 Fiber tracts determined by diffusion tensor imaging and superimposed on a T_2-weighted image. The tracts shown in red and yellow are cortico-spinal tracts; those shown in blue are optic radiations. The lateral geniculate nucleus is shown in green (Image provided courtesy of Dr. Josh Shimony and Mr. Adrian Epstein)

of clinical situations and requires that at least six directionally independent diffusion measurements are made to create this three-vector representation of the diffusion ellipsoid. However, this representation may not suffice for voxels with more complex white matter structure. For example, if two WM tracts cross at 90°, the resultant ellipsoid for this voxel would have a pancake shape, with the plane of the pancake corresponding to the plane of the crossing fibers (remember that the three-vector approach can only describe shapes resembling spheres, rugby balls, and pancakes). Clearly, it would be difficult to follow one of the fiber tracts through such a voxel. Approaches to overcome this limitation are currently under development by several research groups. For example, if diffusion measurements are made in more than six directions [studies with up to 126 directions have been published! (Tuch et al. 2002)], it is possible to apply more sophisticated forms of analysis; in essence, generating shapes more complex than simple ellipsoids. Examples of approaches allowing for more complex shapes include q-space imaging (Tuch 2004; Cohen and Assaf 2002) and spherical harmonic decomposition (Frank 2002). For the example of fiber tracts crossing at 90° given above, a three-dimensional representation of water displacements might look like a cross.

3.5 Diffusion of Molecules Other than ^1H_2O

Though a detailed discussion of these measurements is beyond the scope of this chapter, it is worth noting that it is possible to measure diffusion of molecules other than water. Whereas the concentration of water ^1H in tissues is on the order of 100 M, other metabolites are present in mM concentrations. As a result, these measurements are typically made at much lower spatial resolution than diffusion measurements for water. One advantage of measuring diffusion of molecules other than water is that

these molecules can provide both compartmental and cell-type specificity, which is difficult to achieve in measures of water diffusion. For example, the ADC of the metabolite N-acetyl aspartate, which is present in the intracellular space of neurons but not glia and detected by ^{1}H spectroscopy, has been shown to decrease in association with stroke (Wick et al. 1995). Measurements of the diffusion of intracellular ions ^{23}Na (Goodman et al. 2005) and ^{133}Cs (Goodman et al. 2008) show similar changes in diffusion with injury. Finally, it is possible to exogenously administer markers, such as ^{19}F-fluorodeoxyglucose, into a specific compartment and measure its diffusion (Duong et al. 1998).

3.6 Conclusion

Diffusion sensitive MRI is a mainstay of MR imaging in both clinical and research settings. The method provides a wealth of information about the central nervous system. ADC values are a sensitive and early indicator of tissue injury. Diffusion anisotropy reflects underlying tissue microstructure. It has been employed for (1) evaluating the "health" of white matter, (2) following the course of white matter tracts, and (3) assessing cortical grey matter maturity in developing brain.

References

Armitage PA, Bastin ME (2000) Selecting an appropriate anisotropy index for displaying diffusion tensor imaging data with improved contrast and sensitivity. Magn Reson Med 44(1):117–121

Ay H, Buonanno FS, Schaefer PW, Le DA, Wang B, Gonzalez RG, Koroshetz WJ (1998) Posterior leukoencephalopathy without severe hypertension: utility of diffusion-weighted MRI. Neurology 51(5):1369–1376

Basser PJ, Pajevic S, Pierpaoli C, Duda J, Aldroubi A (2000) In vivo fiber tractography using DT-MRI data. Magn Reson Med 44(4):625–632

Busch E, Hoehn-Berlage M, Eis M, Gyngell ML, Hossman KA (1995) Simultaneous recording of EEG, DC potential and diffusion-weighted NMR imaging during potassium induced cortical spreading depression in rats. NMR Biomed 8(2):59–64

Butts K, Daniel BL, Chen L, Bouley DM, Wansapura J, Maier SE, Dumoulin C, Watkins R (2003) Diffusion-weighted MRI after cryosurgery of the canine prostate. Magnetic resonance imaging. J Magn Reson Imaging 17(1):131–135

Cohen Y, Assaf Y (2002) High b-value q-space analyzed diffusion-weighted MRS and MRI in neuronal tissues – a technical review. NMR Biomed 15(7–8):516–542

Conturo TE, Lori NF, Cull TS, Akbudak E, Snyder AZ, Shimony JS, McKinstry RC, Burton H, Raichle ME (1999) Tracking neuronal fiber pathways in the living human brain. Proc Natl Acad Sci USA 96(18):10422–10427

Copen WA, Schwamm LH, Gonzalez RG, Wu O, Harmath CB, Schaefer PW, Koroshetz WJ, Sorensen AG (2001) Ischemic stroke: effects of etiology and patient age on the time course of the core apparent diffusion coefficient. Radiology 221(1):27–34

Dijkhuizen RM, Knollema S, van der Worp HB, Ter Horst GJ, De Wildt DJ, Berkelbach van der Sprenkel JW, Tulleken KA, Nicolay K (1998) Dynamics of cerebral tissue injury and perfusion after temporary hypoxia-ischemia in the rat: evidence for region-specific sensitivity and delayed damage. Stroke 29(3):695–704

Dijkhuizen RM, de Graaf RA, Tulleken KA, Nicolay K (1999) Changes in the diffusion of water and intracellular metabolites after excitotoxic injury and global ischemia in neonatal rat brain. J Cereb Blood Flow Metab 19(3):341–349

Duong TQ, Ackerman JJH, Ying HS, Neil JJ (1998) Evaluation of extra- and intracellular apparent diffusion in normal and globally ischemic rat brain via ^{19}F NMR. Magn Reson Med 40(1):1–13

Frank LR (2002) Characterization of anisotropy in high angular resolution diffusion-weighted MRI. Magn Reson Med 47(6):1083–1099

Goldberg-Zimring D, Mewes AU, Maddah M, Warfield SK (2005) Diffusion tensor magnetic resonance imaging in multiple sclerosis. J Neuroimaging 15(4 Suppl):68S–81S

Goodman JA, Kroenke CD, Bretthorst GL, Ackerman JJ, Neil JJ (2005) Sodium ion apparent diffusion coefficient in living rat brain. Magn Reson Med 53(5):1040–1045

Goodman JA, Ackerman JJ, Neil JJ (2008) Cs + ADC in rat brain decreases markedly at death. Magn Reson Med 59(1):65–72

Hamstra DA, Chenevert TL, Moffat BA, Johnson TD, Meyer CR, Mukherji SK, Quint DJ, Gebarski SS, Fan X, Tsien CI, Lawrence TS, Junck L, Rehemtulla A, Ross BD (2005) Evaluation of the functional diffusion map as an early biomarker of time-to-progression and overall survival in high-grade glioma. Proc Natl Acad Sci USA 102(46):16759–16764

Heemskerk AM, Drost MR, van Bochove GS, van Oosterhout MF, Nicolay K, Strijkers GJ (2006) DTI-based assessment of ischemia-reperfusion in mouse skeletal muscle. Magn Reson Med 56(2):272–281

Hinchey J, Chaves C, Appignani B, Breen J, Pao L, Wang A, Pessin MS, Lamy C, Mas JL, Caplan LR (1996) A reversible posterior leukoencephalopathy syndrome. N Engl J Med 334(8):494–500

Huppi PS, Maier SE, Peled S, Zientara GP, Barnes PD, Jolesz FA, Volpe JJ (1998) Microstructural development of human newborn cerebral white matter assessed in vivo by diffusion tensor magnetic resonance imaging. Pediatr Res 44(4):584–590

Ito J, Marmarou A, Barzo P, Fatouros P, Corwin F (1996) Characterization of edema by diffusion-weighted imaging in experimental traumatic brain injury. J Neurosurg 84(1):97–103

Kanaan RA, Kim JS, Kaufmann WE, Pearlson GD, Barker GJ, McGuire PK (2005) Diffusion tensor imaging in schizophrenia. Biol Psychiatry 58(12):921–929

Klingberg T, Hedehus M, Temple E, Salz T, Gabrieli JD, Moseley ME, Poldrack RA (2000) Microstructure of temporo-parietal white matter as a basis for reading ability: evidence from diffusion tensor magnetic resonance imaging. Neuron 25(2):493–500

Kroenke CD, Van Essen DC, Inder TE, Rees S, Bretthorst GL, Neil JJ (2007) Microstructural changes of the baboon cerebral cortex during gestational development reflected in magnetic resonance imaging diffusion anisotropy. J Neurosci 27(46):12506–12515

Li F, Han SS, Tatlisumak T, Liu KF, Garcia JH, Sotak CH, Fisher M (1999) Reversal of acute apparent diffusion coefficient abnormalities and delayed neuronal death following transient focal cerebral ischemia in rats. Ann Neurol 46(3):333–342

Li F, Silva MD, Liu KF, Helmer KG, Omae T, Fenstermacher JD, Sotak CH, Fisher M (2000) Secondary decline in apparent diffusion coefficient and neurological outcomes after a short period of focal brain ischemia in rats. Ann Neurol 48(2):236–244

Lin SP, Song SK, Miller JP, Ackerman JJ, Neil JJ (2001) Direct, longitudinal comparison of (1)H and (23)Na MRI after transient focal cerebral ischemia. Stroke 32(4):925–932

Liu AS, Xie JX (2003) Functional evaluation of normothermic ischemia and reperfusion injury in dog kidney by combining MR diffusion-weighted imaging and Gd-DTPA enhanced first-pass perfusion. J Magn Reson Imaging 17(6):683–693

McKinstry RC, Mathur A, Miller JP, Ozcan AO, Snyder AZ, Schefft GL, Almli CR, Shiran SI, Conturo TE, Neil JJ (2002a) Radial organization of developing human cerebral cortex revealed by non-invasive water diffusion anisotropy MRI. Cereb Cortex 12(12):1237–1243

McKinstry RC, Miller JH, Snyder AZ, Mathur A, Schefft GL, Almli CR, Shimony JS, Shiran SI, Neil JJ (2002b) A prospective, longitudinal diffusion tensor imaging study of brain injury in newborns. Neurology 59(6):824–833

Moffat BA, Chenevert TL, Meyer CR, McKeever PE, Hall DE, Hoff BA, Johnson TD, Rehemtulla A, Ross BD (2006) The functional diffusion map: an imaging biomarker for the early prediction of cancer treatment outcome. Neoplasia 8(4):259–267

Moseley ME, Cohen Y, Mintorovitch J, Chileuitt L, Shimizu H, Kucharczyk J, Wendland MF, Weinstein PR (1990) Early detection of regional cerebral ischemia in cats: Comparison of diffusion- and T_2-weighted MRI and spectroscopy. Magn Reson Med 14(2):330–346

Mukherjee P, Bahn MM, McKinstry RC, Shimony JS, Cull TS, Akbudak E, Snyder AZ, Conturo TE (2000) Differences between gray matter and white matter water diffusion in stroke: diffusion-tensor MR imaging in 12 patients. Radiology 215(1):211–220

Mukherjee P, Miller JH, Shimony JS, Philip JV, Nehra D, Snyder AZ, Conturo TE, Neil JJ, McKinstry RC (2002) Diffusion-tensor MR imaging of gray and white matter development during normal human brain maturation. AJNR Am J Neuroradiol 23(9):1445–1456

Neil JJ, Duong TQ, Ackerman JJH (1996) Evaluation of intracellular diffusion in normal and globally ischemic rat brain *via* ^{133}Cs NMR. Magn Reso Med 35(3):329–335

Neil JJ, Shiran SI, McKinstry RC, Schefft GL, Snyder AZ, Almli CR, Akbudak E, Aaronovitz JA, Miller JP, Lee BCP, Conturo TE (1998) Normal brain in human newborns: apparent diffusion coefficient and diffusion anisotropy measured using diffusion tensor imaging. Radiology 209(1):57–66

Neil JJ, Miller JP, Mukherjee P, Huppi PS (2002) Diffusion tensor imaging of normal and injured developing human brain. NMR Biomed 15(7–8):543–552

Oppenheim C, Stanescu R, Dormont D, Crozier S, Marro B, Samson Y, Rancurel G, Marsault C (2000) False-negative diffusion-weighted MR findings in acute ischemic stroke. AJNR Am J Neuroradiol 21(8):1434–1440

Rother J, deCrespigny AJ, D'Arceuil H, Moseley ME (1996) MR detection of cortical spreading depression immediately after focal ischemia in the rat. J Cereb Blood Flow Meta 16(2): 214–220

Schlaug G, Siewert B, Benfield A, Edelman RR, Warach S (1997) Time course of the apparent diffusion coefficient (ADC) abnormality in human stroke. Neurology 49(1):113–119

Silva M, Omae T, Helmer K, Li F, Fisher M, Sotak C (2002) Separating changes in the intra- and extracellular water apparent diffusion coefficient following focal cerebral ischemia in the rat brain. Magn Reson Med 48(5):826–837

Song SK, Sun SW, Ramsbottom MJ, Chang C, Russell J, Cross AH (2002) Dysmyelination revealed through MRI as increased radial (but unchanged axial) diffusion of water. Neuroimage 17(3):1429–1436

Song SK, Yoshino J, Le TQ, Lin SJ, Sun SW, Cross AH, Armstrong RC (2005) Demyelination increases radial diffusivity in corpus callosum of mouse brain. Neuroimage 26(1):132–140

Sun SW, Liang HF, Le TQ, Armstrong RC, Cross AH, Song SK (2006) Differential sensitivity of in vivo and ex vivo diffusion tensor imaging to evolving optic nerve injury in mice with retinal ischemia. Neuroimage 32(3):1195–1204

Takano K, Latour LL, Formato JE, Carano RAD, Helmer KG, Hasegawa Y, Sotak CH, Fisher M (1996) The role of spreading depression in focal ischemia evaluated by diffusion mapping. An Neurol 39(3):308–318

Tuch DS (2004) Q-ball imaging. Magn Reson Med 52(6):1358–1372

Tuch DS, Reese TG, Wiegell MR, Makris N, Belliveau JW, Wedeen VJ (2002) High angular resolution diffusion imaging reveals intravoxel white matter fiber heterogeneity. Magn Reson Med 48(4):577–582

Wick M, Nagatomo Y, Prielmeier F, Frahm J (1995) Alteration of intracellular metabolite diffusion in rat brain *in vivo* during ischemia and reperfusion. Stroke 26(10):1930–1933

Wimberger DM, Roberts TP, Barkovich AJ, Prayer LM, Moseley ME, Kucharczyk J (1995) Identification of "premyelination" by diffusion-weighted MRI. J Comput Assis Tomogr 19(1):28–33

Woodward LJ, Anderson PJ, Austin NC, Howard K, Inder TE (2006) Neonatal MRI to predict neurodevelopmental outcomes in preterm infants. N Engl J Med 355(7):685–694

Xue R, van Zijl PCM, Crain BJ, Solaiyappan M, Mori S (1999) In vivo three-dimensional reconstruction of rat brain axonal projections by diffusion tensor imaging. Magn Reson Med 42(6):1123–1127

Zhong J, Petroff OAC, Prichard JW, Gore JC (1993) Changes in water diffusion and relaxation properties of rat cerebrum during status epilepticus. Magn Reson Med 30(2):241–246